Journal of Power Sources 246 (2014) 74–83

Contents lists available at ScienceDirect

Journal of Power Sources

journal homepage: www.elsevier.com/locate/jpowsour

A new alkali-resistant Ni/Al_2O_3-MSU-1 core–shell catalyst for methane steam reforming in a direct internal reforming molten carbonate fuel cell

Jian Zhang [a], Xiongfu Zhang [a,*], Weifeng Liu [a], Haiou Liu [a], Jieshan Qiu [a,1], King Lun Yeung [b]

[a] State Key Laboratory of Fine Chemicals, School of Chemical Engineering, Dalian University of Technology, Dalian 116024, PR China
[b] Department of Chemical and Biomolecular Engineering, The Hong Kong University of Science and Technology, Clear Water Bay, Kowloon, Hong Kong Special Administrative Region

HIGHLIGHTS

- An alkali-resistant core–shell catalyst with mesoporous MSU-1 shell was prepared for a DIR-MCFC system.
- The core–shell catalysts with different thickness shells could be obtained by finely adjusting the loading NaF amount.
- The core–shell catalyst displays better activity than the one with microporous Sil-1 shell for DIR-MCFC system.

GRAPHICAL ABSTRACT

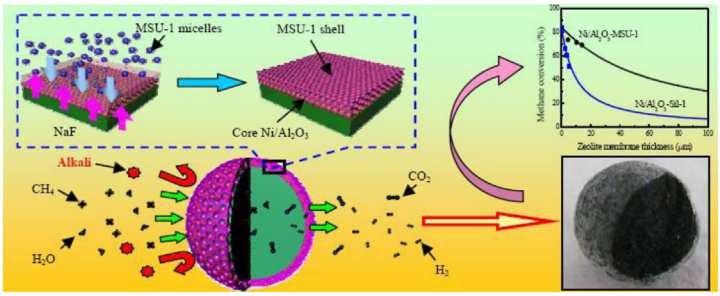

ARTICLE INFO

Article history:
Received 16 June 2013
Accepted 11 July 2013
Available online 26 July 2013

Keywords:
Core–shell structure
Molecular sieve membrane
Methane steam reforming
Catalyst deactivation
Fuel cell

ABSTRACT

An alkali-resistant catalyst for direct internal reforming molten carbonate fuel cell (DIR-MCFC) is prepared by growing a thin shell of mesoporous MSU-1 membrane on Ni/Al_2O_3 catalyst beads. The MSU-1 shell is obtained by first depositing a monolayer of colloidal silicalite-1 (Sil-1) on the catalyst bead as linkers and then using NaF stored in the beads to catalyze the growth of the MSU-1 layer. The resulting core–shell catalysts display excellent alkali-resistance and deliver stable methane conversion and hydrogen yield in an out-of-cell test simulating the operating conditions of an operating DIR-MCFC. Higher conversion and yield (i.e., up to over 70%) are obtained from the new core–shell catalyst with MSU-1 shell compared to the catalyst with microporous Sil-1 shell. A mathematical model of the reaction and poisoning of the core–shell catalyst is used to predict the optimum shell thickness for its reliable use in a DIR-MCFC.

1. Introduction

Core–shell catalysts with molecular sieve and zeolite shells have been employed in various applications to enhance product selectivity and yield, and to mitigate catalyst poisoning [1]. Tsubaki and coworkers [2–7] prepared Co/SiO_2 core with a ZSM-5 shell catalysts for Fischer–Tropsch synthesis reaction resulting in higher iso-paraffin yields. The zeolite shell is believed to regulate the size and shape of the product molecules that can leave the core–shell catalysts leading to the higher iso-paraffin yield of these catalysts. Kapteijn et al. [8,9] used the zeolite shell instead to regulate the transport of reactants to the core catalyst. Their group employed a thin Sil-1 shell on Pd/TiO_2 to selectively permeate 1-hexene from

* Corresponding author. Tel./fax: +86 411 84986155.
E-mail addresses: xfzhang@dlut.edu.cn (X. Zhang), jqiu@dlut.edu.cn (J. Qiu).
[1] Tel./fax: +86 411 84986080.

0378-7753/$ – see front matter © 2013 Elsevier B.V. All rights reserved.
http://dx.doi.org/10.1016/j.jpowsour.2013.07.075

mixtures containing 3,3-dimethylbut-1-ene (3,3-DMB), and carry out highly selective hydrogenation of 1-hexene. Similar enhanced selectivity was reported by Khan and coworkers [10] using a Ni/SiO_2 core with Sil-1 shell catalyst.

Nonuniform catalyst distributions (e.g., egg yolk) have been used in catalysis and membranes to avoid poisoning of active sites during reaction [11–13]. Core–shell catalysts can mitigate catalyst poisoning by using the zeolite shell as a transport barrier against poisons. Ni/Al_2O_3 core with Sil-1 shell catalyst was used in our prior works [14,15] as methane steam reforming catalyst in the DIR-MCFC. The Sil-1 zeolite shell protects the nickel catalyst from the alkali vapor and electrolyte solution, and prevents rapid catalyst poisoning. However, the transport resistance across the narrow zeolite pores (ca. 0.5 nm) resulted in lower methane conversion. In order to address this shortcoming, this work investigates the preparation and performance of a mesoporous molecular sieve (MSU-1) as a protective shell for the methane steam reforming Ni/Al_2O_3 catalyst for DIR-MCFC.

MSU-1 molecular sieve is mesoporous silica with three dimensional, interconnecting, worm-like pores of ca. 6.6 nm in diameter [16,17]. Besides having a large surface area, MSU-1 can tolerate harsh thermal and hydrothermal conditions [18,19]. Several synthesis methods for MSU membranes have been reported [20–26]. Boissière and coworkers [25,26] were able to prepare low defect MSU membrane using a nonionic surfactant as template and NaF as catalyst to catalyze silica condensation. This work will examine the synthesis and growth of MSU-1 shell on high curvature surface of Ni/Al_2O_3 beads using Sil-1 nanocrystals as surface linkers and pre-impregnated NaF as catalyst. The growth of the MSU shell and the characterization of its physicochemical and thermomechanical properties were performed with the objective of obtaining an improved alkali-resistant, core–shell catalysts for use in DIR-MCFC.

2. Experimental

2.1. Preparation Ni/Al_2O_3 catalyst

The detailed description of materials and methods for preparing Ni/Al_2O_3 catalysts was reported in a prior work [14]. The γ-Al_2O_3 beads (0.85–1.7 mm) were purchased from Dalian Haixin Chemical Ltd. and have a specific surface area of 300 $m^2\ g^{-1}$ and pore volume of 0.42 $cm^3\ g^{-1}$. The beads were rinsed in deionized distilled water and calcined at 523 K for 5 h. An incipient wetness impregnation method was used to prepare the Ni/Al_2O_3 with 12.5 wt.% nickel oxide loading from a 4 wt.% aqueous solution of nickel nitrate hexahydrate (AR, Kermel). The Ni/Al_2O_3 catalysts were dried at 373 K for 12 h, before air calcination in a furnace at 923 K for 4 h. The catalysts were stored for latter characterization and use.

2.2. Preparation Ni/Al_2O_3 core and MSU-1 shell catalysts

The procedure for preparing the core–shell catalysts is illustrated in Fig. 1. Sil-1 nanocrystals were used as linkers for the deposition and growth of MSU-1 on the bead surface (Fig. 1a). The 160 ± 10 nm Sil-1 crystals were deposited on the surface of the Ni/Al_2O_3 catalyst beads using organic linkers according to the methods reported in prior works [14,15,27]. The beads were then impregnated with NaF to catalyze MSU growth. A gram of the seeded Ni/Al_2O_3 beads were immersed in 20 ml 0.1–0.4 wt. % NaF solution. The solution was placed in an oven at 323 K for 24 h to evaporate the water. The beads were weighed to determine the NaF weight loading.

The MSU-1 shell was grown on the Sil-1 modified and NaF-impregnated Ni/Al_2O_3 catalyst beads from a synthesis solution with molar composition of 1 SiO_2:0.1 Brij-35:10 EtOH:100H_2O:x NaF (x = 0.02–0.08). The synthesis solution was prepared by dissolving 5.3 g Brij-35 (high purity grade, Amresco) in a solution of 16.2 ml ethanol and 80 ml deionized distilled water, followed by the addition of 8.8 ml tetraethyl orthosilicate (TEOS, AR, Kermel). The synthesis solution was aged at room temperature for 24 h, and the pH was adjusted to 7, prior to use in order to avoid the dissolution of nickel from the catalyst beads. A gram of the seeded and NaF-impregnated catalyst beads was added to the prepared solution, and the synthesis was carried out in a rotating Teflon-lined autoclave (5 rpm) at 313 K. After synthesis, the catalyst beads were washed with deionized distilled water, then dried in air at 333 K for 12 h before calcining at 873 K for 6 h to remove the organic template molecules.

A Ni/Al_2O_3 core and MSU-1 shell catalyst (Ni/Al_2O_3-MSU-1-B) was also prepared on Ni/Al_2O_3 catalyst beads without the Sil-1 crystals as linkers to investigate the role of the Sil-1 crystals in MSU-1 shell deposition and growth (Fig. 1b). A Ni/Al_2O_3 core and Sil-1 shell catalyst (Ni/Al_2O_3-Sil-1) was also prepared for comparison. The same procedure as in prior report [14,15] was used to prepare the catalyst.

2.3. Catalyst characterization

The catalysts were examined under electron microscopes (JSM-6360LV SEM and Philips CM30T TEM) to monitor the deposition and growth of the MSU-1 shell on the catalyst beads. Samples of the MSU-1 shells were analyzed by D/Max 2400 Rigaku X-ray diffractometer (XRD) equipped with Cu Kα radiation source (λ = 0.1542 nm) and operated at a voltage of 40 kV and 50 mA. Nitrogen adsorption–desorption isotherms were measured by Micromeritics 2010 porosimeter at 77.5 K after outgassing the sample under vacuum at 523 K for 5 h. The specific surface area was

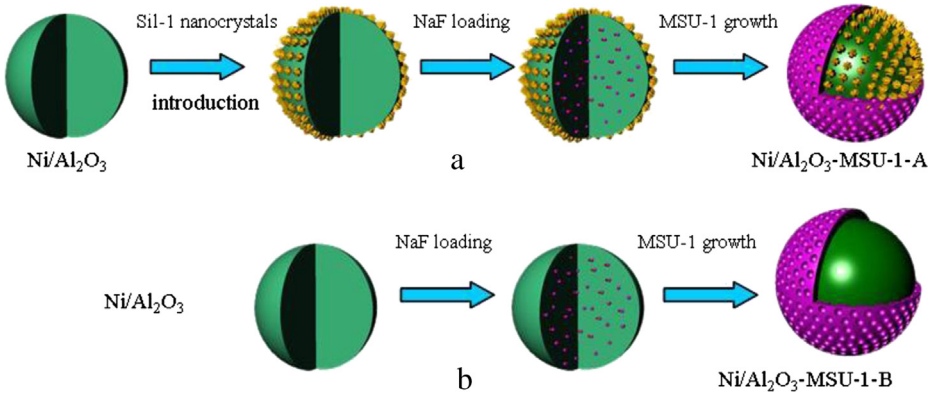

Fig. 1. Synthesis process of the core–shell catalysts with (a) and without Sil-1 crystals as linkers (b).

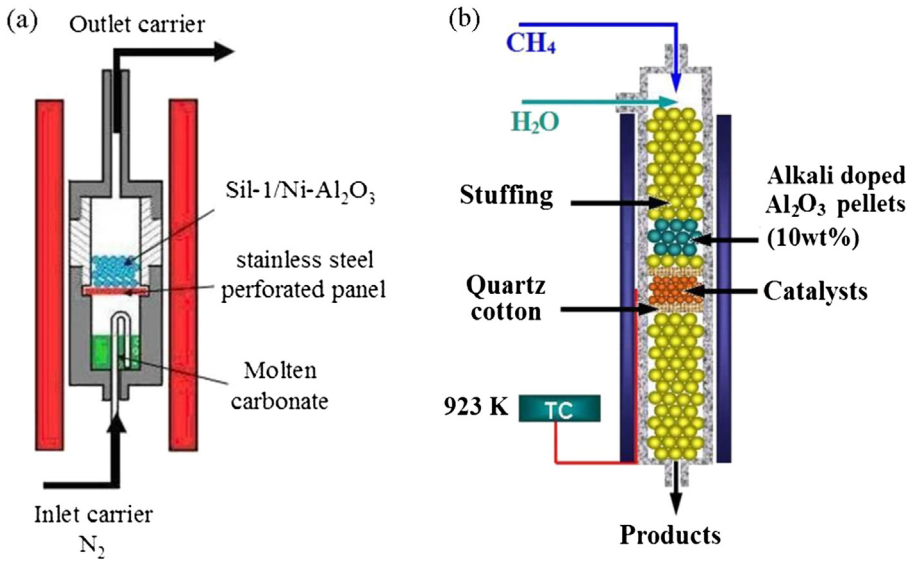

Fig. 2. Schematic drawings of the treatment and reactor set-ups for: (a) exposure of catalyst to alkali vapor; (b) methane steam reforming under alkali vapor.

determined by BET method, while the pore size distribution was calculated by Dollimore–Heal (DH) method [28].

2.4. Catalytic methane steam reforming reaction

The tolerance of the core–shell catalysts against alkali vapor was measured using two methods. Method 1 exposed the catalyst to alkali vapor before reaction in the setup shown in Fig. 2a. 1.2 g of catalyst beads were exposed to alkali vapor that was generated by bubbling nitrogen gas through 4 g of molten electrolytes (ca. 62 mol. % Li_2CO_3 and 38 mol. % K_2CO_3) kept at 923 K. The catalysts were then transferred to a packed bed reactor and used for methane reforming reaction. Method 2 used the reactor setup shown in Fig. 2b to simulate the conditions found in DIR-MCFC. The stainless steel reactor had a diameter of 8 mm and a length of 400 mm. A 0.8 g of catalysts was placed in a reactor downstream from alumina pellets saturated with 4 g of the electrolyte (62 mol. % Li_2CO_3, 38 mol. % K_2CO_3). The catalysts had been first reduced in 40 sccm H_2 at 923 K for 4 h to convert the nickel oxide to nickel metal before switching the flow to a 20 sccm reactant feed mixture of CH_4:3H_2O. The hot gases flowed through the beads saturated with electrolytes generating alkali vapor before flow passed the catalyst. The reaction was monitored by an on-line gas chromatograph (GC 7890T) equipped with a TCD detector (200 mm length × 3 mm diameter, TDX-01, Shanghai Techcomp Ltd) and using argon as carrier gas.

A mathematical model was developed based on the experimental data to examine the effects of the shell thickness and materials (i.e., MSU-1 and Sil-1) on alkali poisoning during the methane steam reforming reaction [14]. Table 1 lists the numerical values for the modeling parameters for the core–shell catalyst.

3. Results and discussion

3.1. Core–shell catalysts

The pictures of the Ni/Al_2O_3-MSU-1-A, Ni/Al_2O_3-MSU-1-B and Ni/Al_2O_3-Sil-1 core–shell catalyst beads are shown in Fig. 3a–c, with the corresponding high magnification electron microscopy images shown in Fig. 3d and f. Comparing Ni/Al_2O_3-MSU-1-A and Ni/Al_2O_3-MSU-1-B core–shell catalysts clearly shows that the Sil-1 linkers are essential for the adhesion of the MSU-1 shell on the catalyst bead. It can be seen in Fig. 3a that a white MSU-1 shell uniformly cladded the bluish Ni/Al_2O_3 beads in Ni/Al_2O_3-MSU-1-A, while the MSU-1 formed an uneven coating on the Ni/Al_2O_3-MSU-1-B as shown in Fig. 3b. Sil-1 also grew into a uniform shell around the seeded Ni/Al_2O_3-Sil-1 beads as shown in Fig. 3c. It is clear from the results that MSU-1 and Sil-1 deposited to form thin but well intergrown layers on the seeded Ni/Al_2O_3 beads (see Fig. 3d and f insets). Inspection under microscope indicates that the shells are free of cracks and defects. On the other hand, the shell was poorly formed on Ni/Al_2O_3-MSU-1-B (cf. Fig. 3e) with uneven thickness and bare patches.

It is speculated that for the deposition and growth of MSU-1 shell the Sil-1 crystal layer acted both as a diffusion barrier against contamination from the catalyst bead and as an adhesion layer for MSU-1. The monolayer of Sil-1 crystals was attached to the bead surface by an organic linker not unlike the methods used to prepare defect-free membranes and films [29–34]. The nanocrystals were then sintered and stabilized on the bead surface by a heat treatment. The nanocrystals present a surface rich in hydroxyl groups for anchoring the growth of MSU-1. The Sil-1 layer is clearly

Table 1
Numerical values of modeling parameters.

Parameters	Symbol	Value	Unit
Gas volumetric feed rate	v	3.33×10^{-6}	$m^3\ s^{-1}$
Temperature	T	923	K
Pressure	P	101325	Pa
Steam to carbon molar feed ratio	$y_{CH_4,o}$	3	–
Methane molar feed rate	$F_{CH_4,0}$	4.40×10^{-6}	mol s^{-1}
Catalyst mass	m_{cat}	0.0008	kg
Mass transfer coefficient for methane through core catalyst[a]	$K_{CH_4,A}$	2314	kg^{-1}
Diffusivity of methane through MSU-1 shell	$D_{CH_4,\ MSU-1}$	5.65×10^{-5}	m kg^{-1}
Modified equilibrium constant between bulk gas and catalyst pore for catalyst (without shell)	$K'_{P,A1}$	0.8	s^{-1}
Proportionality constant	β	2.68×10^{-4}	–

[a] The diffusivity value was based on the data from the reference [14].

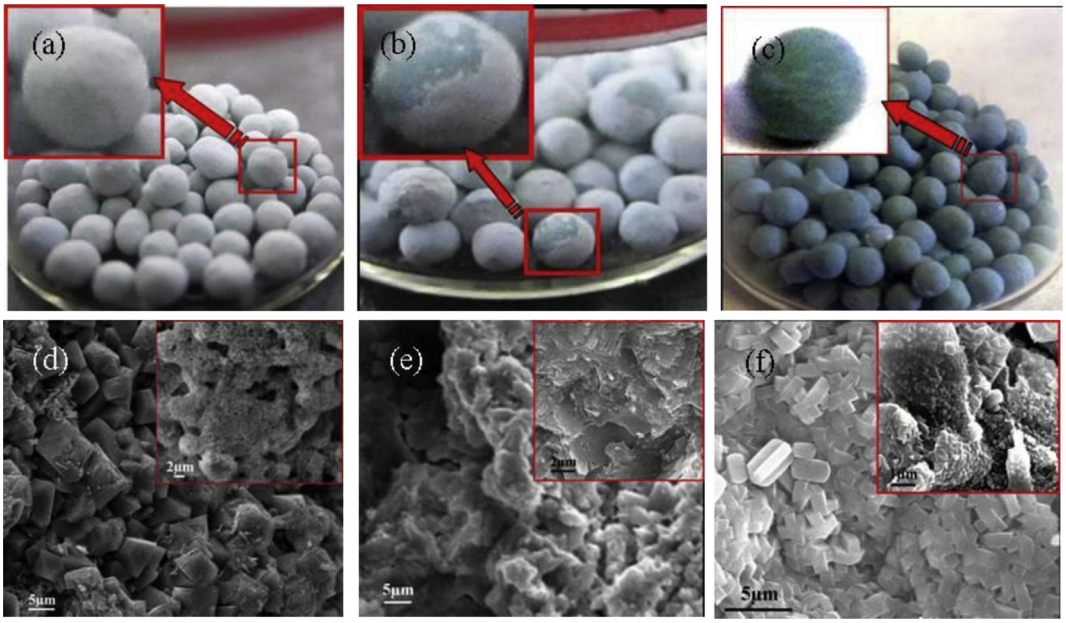

Fig. 3. Pictures and the corresponding high magnification images of the samples: (a, d) Ni/Al_2O_3-MSU-1-A; (b, e) Ni/Al_2O_3-MSU-1-B; (c, f) Ni/Al_2O_3-Sil-1.

apparent in Fig. 3d, and appears unaffected by the synthesis and deposition of MSU-1. Also, the Sil-1 crystals can alter the composition and chemistry of the bead surface, which had in numerous occasions shown to be critical for the growth of molecular sieve membranes [35–38]. Indeed, Pinnavaia's group had proposed a seed-induction mechanism for the synthesis of MSU-1 powders and membranes using zeolite seeds (i.e., ZMS-5, zeolite beta and Y) [20,39]. Accordingly, the Sil-1 seeds of Ni/Al_2O_3-MSU-1-A provide nucleation sites for MSU-1 crystallization and growth on the bead surface. The seeds also served to moderate the difference between the expansion coefficients between support and MSU-1 layer [40].

3.1.1. Growth of MSU-1 on high curvature surface

The deposition of a mesoporous shell on a high curvature surface is difficult as the strains can lead to defects and cracks. Furthermore, the beads being made of coarse sintered alumina powder have rough and uneven surface (Fig. 4a and b). Seeding the bead with a layer of Sil-1 had the effect of smoothing out the surface and decreasing the size of surface pores as shown in Fig. 4c. NaF was impregnated into the seeded beads to localize the growth of MSU-1 and avoid bulk crystallization in the solution. NaF catalyzes silica condensation and promotes MSU-1 deposition and growth [17,41]. Poor deposition and growth were observed on beads without NaF, while bulk precipitation and uneven shell formation were obtained when NaF was added directly to the synthesis mixture. Fig. 4d–f document in a series of SEM images which are the progression of MSU-1 deposition and growth into a shell around the catalyst beads.

Fig. 4d shows the depositions of micron and submicron-sized particles on the surface of the seeded catalyst beads after 2 h of synthesis. The particles uniformly clad the surface of the bead (cf. Fig. 4d inset). It should be noted that the particles display prismatic shape that could be described as being of a double quadrangular pyramidal shape. The particles grew in size with synthesis as shown in Fig. 4e. The particle shape changes to tetrakaidecahedron shape that consists of eight hexagonal and six quadrate faces. The deposited layer appears denser with evidence of intergrowth between particles as shown by the inset in Fig. 4e. A 15 μm thick shell was obtained at the end of the synthesis (Fig. 4f). The shell is dense and completely clad the catalyst bead forming the Ni/Al_2O_3-MSU-1-A core shell catalyst.

Samples were taken from Ni/Al_2O_3-MSU-1-A and Ni/Al_2O_3-MSU-1-B by scrapping the surface of the beads. Both samples display a strong X-ray diffraction peak at 1.21° (which can be assigned to a $d_{100} = 75.6$ A) as shown in Fig. 5a that is consistent with the standard X-ray diffraction pattern of MSU-1. This confirms the successfully deposition and growth of MSU-1 on the catalyst beads. The samples were also analyzed by transmission electron microscopy and images taken at high magnification show pores of about 6 nm diameter (cf. Fig. 5b). Closer examination indicates that the samples do have the worm-like random pore network that characterizes MSU-1 [42]. This is further confirmed by the nitrogen physisorption isotherms shown in Fig. 5c. Shell scrapping samples from both Ni/Al_2O_3-MSU-1-A and Ni/Al_2O_3-MSU-1-B display the Type IV isotherm with H2 hysteresis loop of MSU-type material. The pore size distributions calculated by Dollimore-Heal (DH) method are plotted in Fig. 5d showing that the MSU shells of Ni/Al_2O_3-MSU-1-A and Ni/Al_2O_3-MSU-1-B have average pore diameters of 6.3 nm and 7.1 nm, respectively.

3.1.2. Effects of NaF on the growth of MSU-1 shell

Low concentrations of fluoride salts are shown to stabilize the precursor micelles in MSU-1 synthesis [43], while at higher concentrations it catalyzes MSU-1 crystallization. The addition of the fluoride salts (i.e., NaF) to the synthesis promotes the deposition and growth of MSU-1 shell on the catalyst bead as shown in our study. Loading the beads with NaF localized the deposition and growth of MSU-1 on the bead surface and prevented the bulk crystallization and precipitation of MSU-1 particles in the solution. The diffusion of fluoride salts to the bead surface catalyzes MSU-1 crystallization at the interface. However, the NaF concentration on the bead surface decreases as the transport resistance increases with the growth of the MSU-1 shell around the bead and as the stored fluoride salt becomes depleted. Accordingly, the growth of the shell would gradually decreases with time and reaches a limiting layer thickness. Thus, it may be possible to use NaF loading to control the shell thickness.

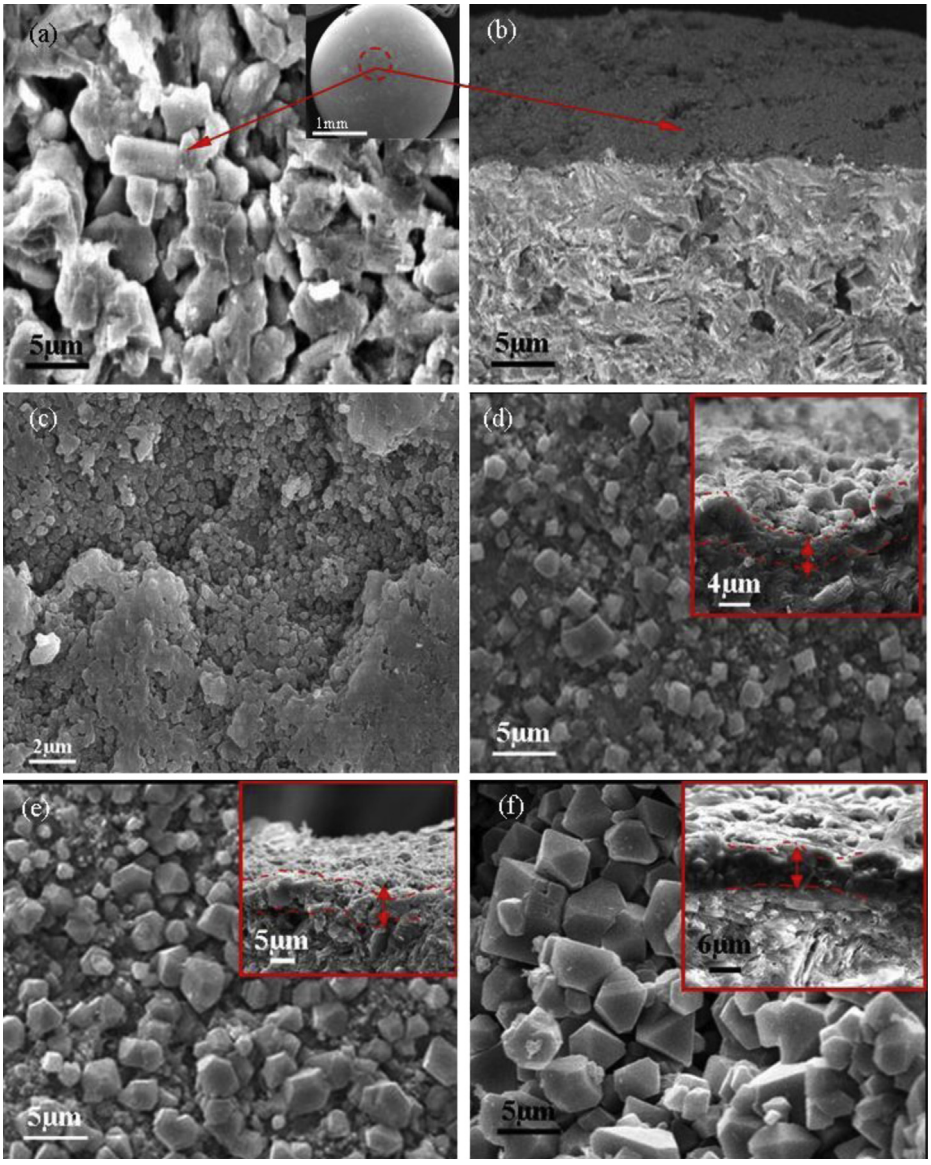

Fig. 4. SEM images of surface and cross section of (a, b) Ni/Al_2O_3, (c) Ni/Al_2O_3 with loaded Sil-1 crystals and Ni/Al_2O_3-MSU-1-A samples with synthesis time of (d) 2 h; (e): 16 h; (f): 24 h (313 K, 1 SiO_2:0.1 Brij-35:10 EtOH:100H_2O:0.08 NaF).

Fig. 6 shows the cross-sections of core–shell catalysts obtained from beads impregnated with different amounts of NaF, but grown from same synthesis solution (1 SiO_2:0.1 Brij-35:10 EtOH:100H_2O) under similar conditions (i.e. 313 K, 24 h, 5 rpm rotation). The MSU-1 shell is observed to be thicker on beads with higher NaF loadings. With increasing the NaF amount loaded in the beads from 0.02 wt.% to 0.08 wt.%, the thickness of the MSU-1 membrane also increases from ca. 2 μm–14 μm. A high NaF loading catalyzes rapid nucleation and growth of the MSU-1 shell. Thus, the synthesis of the MSU-1 membrane with the NaF diffusion allows us to finely tune the thickness of the MSU-1 membrane because the formation of the MSU-1 membrane completely depends on the catalyst amount of NaF.

According to our mathematic model built, the relationship between loading amount of NaF and thickness of MSU-1 shell was calculated as shown in Fig. 6e. It is clearly seen from the plot in Fig. 6e that there is a well one-to-one correspondence between shell thickness and loading amount of NaF. However, the shell thickness increases faster with the amount of NaF at the lower NaF concentration (no more than about 0.2). The maximum thickness can be only up to around 30 μm due to the limit of loading amount of NaF which is determined by the pore volume of the bead. The thickness of the shell should be accurately achieved according to the loading amount of NaF calculated.

A proposed mechanism for the formation MSU-1 shell is illustrated in Fig. 7. The deposited layer of Sil-1 is anchored to the surface of the catalyst beads following a high temperature treatment. This layer provides a more homogeneous surface, both physically and chemically for MSU-1 deposition. It also provides a surface rich in hydroxyl groups believed to be important for the nucleation and growth of MSU-1. Furthermore, this Sil-1 layer serves as a diffusion barrier against contaminants from the catalyst beads and moderates the release of the stored NaF that catalyzes MSU-1 growth. Storing the fluoride salt in the bead localizes the deposition MSU-1 on the surface of the bead and avoids the problem of bulk crystallization from the solution. The fluoride salt diffuses from the bead interior to the surface where it catalyzes MSU-1 deposition and growth. The depletion of the stored salt and

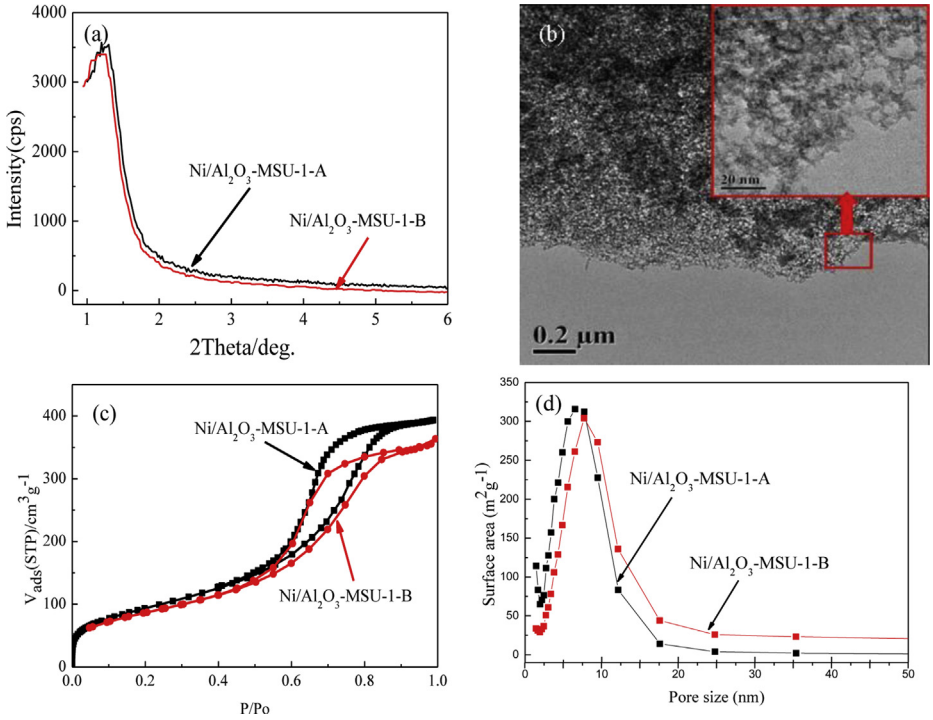

Fig. 5. (a) XRD patterns, (b) TEM images, (c) nitrogen adsorption isotherms, (d) pore size distributions of the shell samples scraped from the core–shell catalysts.

the formation of the mesoporous shell result in a drastic drop in NaF released to the surface. This has the effect of slowing further MSU-1 growth, and therefore regulates the shell thickness of the core–shell catalyst.

3.2. Catalytic methane steam reforming reaction

Prior works [14,15] on Ni/Al_2O_3 core with Sil-1 shell catalyst (Ni/Al_2O_3-Sil-1) demonstrated that core–shell catalyst can mitigate catalyst poisoning by alkali vapor and electrolyte solution during methane steam reforming reaction under conditions that simulate the operation of a DIR-MCFC. However, the transport resistance across the narrow zeolite pores (ca. 0.5 nm) led to a lower methane conversion. This work investigates the possible use of a mesoporous MSU-1 shell to remedy this shortcoming without compromising the resistant of the core–shell catalyst against alkali poisoning.

The methane conversions over the fresh Ni/Al_2O_3 catalyst and the Ni/Al_2O_3-MSU-1-A, Ni/Al_2O_3-MSU-1-B and Ni/Al_2O_3-Sil-1 core–shell catalysts are plotted in Fig. 8a. All four catalysts are stable for methane steam reforming reaction. The Ni/Al_2O_3 catalyst gave a conversion of 84% that is the highest among the four catalysts investigated in the study followed by Ni/Al_2O_3-MSU-1-B with 80% conversion and Ni/Al_2O_3-MSU-1-A with 73% conversion. Ni/Al_2O_3-Sil-1 that has a conversion of 62% is the lowest among the core–shell catalysts despite having the thinnest shell. The progressively lower conversion in the core–shell catalyst is related to the transport resistance across the shell. The mesoporous MSU-1 is more accessible than the microporous Sil-1, and Ni/Al_2O_3-MSU-1-A grown on Sil-1 seeded beads has lesser defects than Ni/Al_2O_3-MSU-1-B grown on bare surface.

The catalysts' activity for methane steam reforming was again measured after their exposure to alkali vapor (treated for 6 h under alkali vapor). Fig. 8b shows that the bare Ni/Al_2O_3 catalyst was completely poisoned and is inactive. The methane conversion over Ni/Al_2O_3-MSU-1-A is 66%, roughly ten percent lower than the fresh catalyst, compared to Ni/Al_2O_3-Sil-1 that suffered a nearly 25% drop in conversion to 50%. Ni/Al_2O_3-MSU-1-B exposed to alkali vapor showed a sharp drop in methane conversion from 80% to 40% due to shell defects in the Ni/Al_2O_3-MSU-1-B resulting in alkali poisoning of the core catalyst. The methane conversion further decreased to about 10% during the 6 h reaction and is believed to be due to alkali intrusion from the salts accumulated on the shell surface during the alkali treatment. The propagation of defects during the high temperature reaction led to cracks and eventual shell delamination of the Ni/Al_2O_3-MSU-1-B as can be seen from the picture of the Ni/Al_2O_3-MSU-1-B recovered after the reaction (cf. Fig. 9a). But Ni/Al_2O_3-MSU-1-A remains the perfect core–shell structure; even after the 6 h of vapor alkali treatment and methane steam reforming reaction (cf. Fig. 9b).

Ni/Al_2O_3-MSU-1-A core–shell catalysts were prepared with shell thicknesses of 2.2, 4.5, 10.7 and 14.1 microns. The catalysts were exposed to alkali vapor before measuring their activity for methane steam reforming reaction. Fig. 10a plots methane conversion as a function of reaction time. The methane conversion on the Ni/Al_2O_3-MSU-1-A catalyst with thin shell (i.e., 2.2 μm) is 40% and is significantly lower than the other core–shell catalysts. This indicates that the shell is too thin and alkali can penetrate through the shell to poison the core catalyst. Core-shell catalysts with thicker shells can effectively protect the core catalyst from alkali poison and are able to maintain a relatively high conversion of 60–65%. The methane steam reforming reaction was conducted in presence of alkali vapor for Ni/Al_2O_3-MSU-1-A and Ni/Al_2O_3-Sil-1 core–shell catalysts according to reaction Method 2. The core–shell catalysts have respectively 10 μm thick Ni/Al_2O_3-MSU-1-A shell, and 3.5 μm thick Sil-1 shells. The alkali vapor was generated upstream, from a bed of alumina pellets saturated with 4 g of the electrolyte (62 mol. % Li_2CO_3, 38 mol. % K_2CO_3). The methane steam reforming reaction on both catalysts was also carried out in the absence of alkali vapor for comparison. Fig. 10b plots the conversion data over 120 h of reaction. The reaction results show that both core–shell catalysts are effective against alkali poisoning during

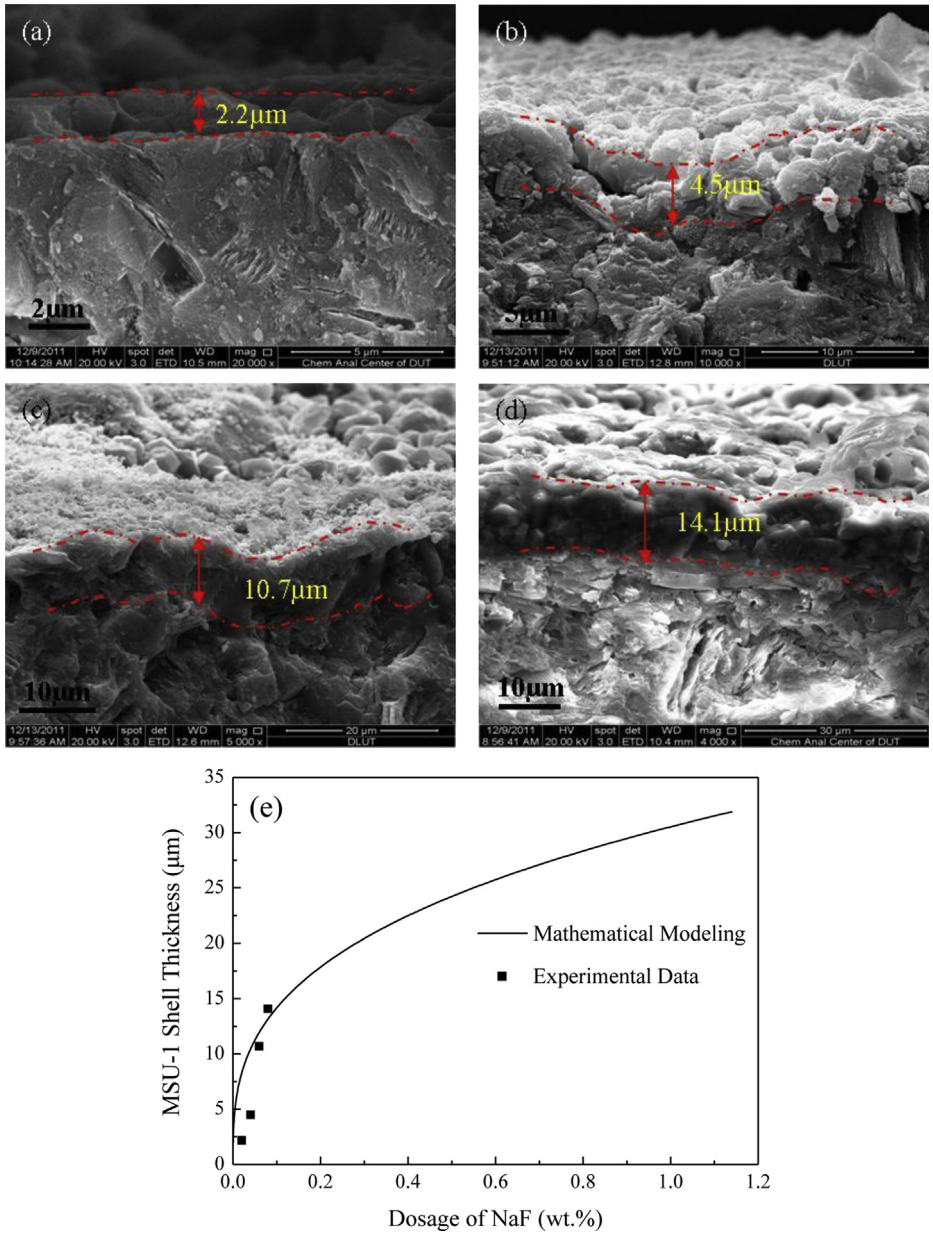

Fig. 6. SEM images of cross sections of the Ni/Al_2O_3-MSU-1-A catalysts with different shell thicknesses using different NaF loading dosages in the Ni/Al_2O_3 beads: 1 (a) 0.02 wt.%; (b) 0.04 wt.%; (c) 0.06 wt.%; (d) 0.08 wt.%. (e) Illustration of the MSU-1 shell thickness with the loading dosage of NaF.

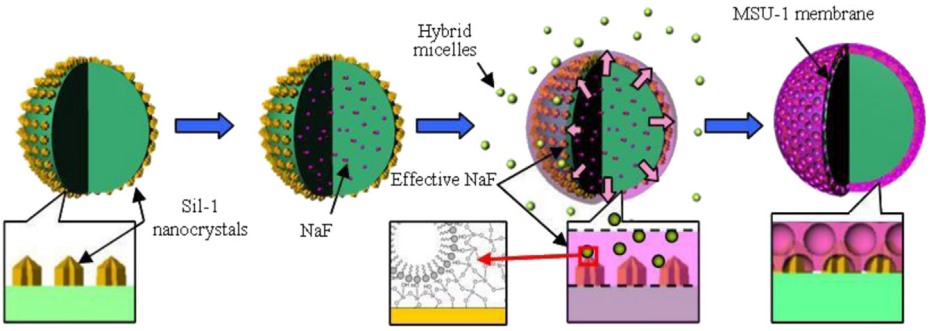

Fig. 7. Schematic illustration of the preparation of MSU-1 membrane on the spherical Ni/Al_2O_3 catalysts via assistance of NaF and Sil-1 nanocrystals.

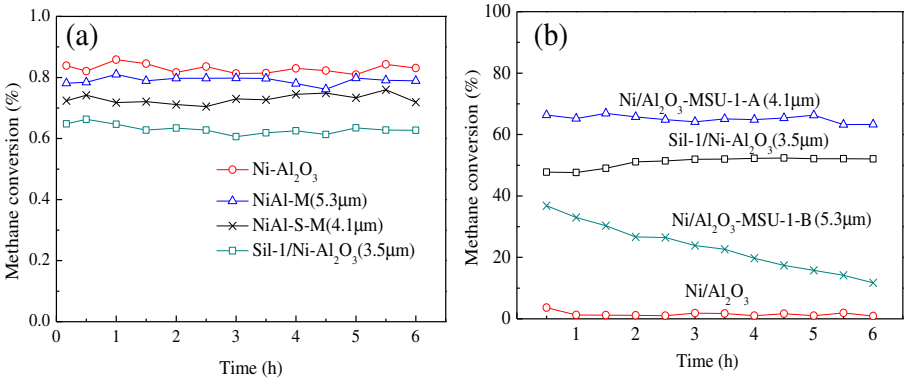

Fig. 8. Catalytic performances of different catalysts for SRM reaction: (a) fresh catalysts; (b) catalysts treated with vapor alkali (Method 1: Poisoning amount of alkali in the 6 h exposure to alkali vapor: 0.31 g).

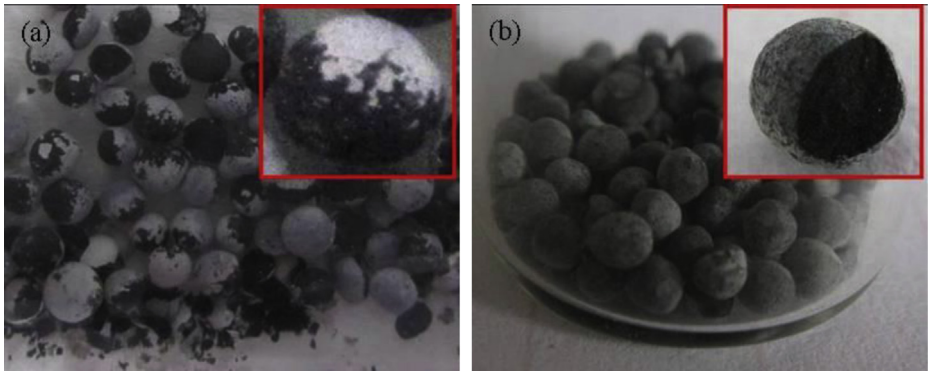

Fig. 9. Pictures of the catalysts treated with vapor alkali (Method 1) and after reaction: (a) Ni/Al_2O_3-MSU-1-B; (b) Ni/Al_2O_3-MSU-1-A.

methane steam reforming reaction under conditions that closely simulate real situation during DIR-MCFC operation. High conversions were obtained from Ni/Al_2O_3-MSU-1-A that has a mesoporous shell despite having a thick shell, while the Ni/Al_2O_3-Sil-1 that has a thin shell (ca. 3.5 μm) displayed significantly low conversions. The reaction study shows that Ni/Al_2O_3-MSU-1-A and Sil-1 shells are sufficient to prevent alkali poisoning, but the high transport resistance of methane across the microporous zeolite shell led to low reaction conversion for the Ni/Al_2O_3-Sil-1 catalyst compared to the new core–shell catalyst.

Fig. 11a compares the methane conversions on fresh Ni/Al_2O_3-MSU-1-A and Ni/Al_2O_3-Sil-1 core–shell catalysts of different shell thicknesses in the absence of alkali poison. Both experimental and simulative results show that for the same thickness, the transport resistance across the microporous Sil-1 zeolite shell is greater than for the mesoporous Ni/Al_2O_3-MSU-1-A shell, and thicker shells have higher transport resistance resulting in lower reaction conversion. The Fig. 11a also shows that there is excellent agreement between mathematical model and experiment. The methane diffusivity across Ni/Al_2O_3-MSU-1-A shell is roughly 6 times that of Sil-1 shell. The mathematical model also correctly predicted the reaction behavior of the Ni/Al_2O_3-MSU-1-A core–shell catalyst during alkali poisoning (Fig. 11b). Rapid poisoning is observed for the Ni/Al_2O_3 catalyst. Without a shell, the catalyst is completely

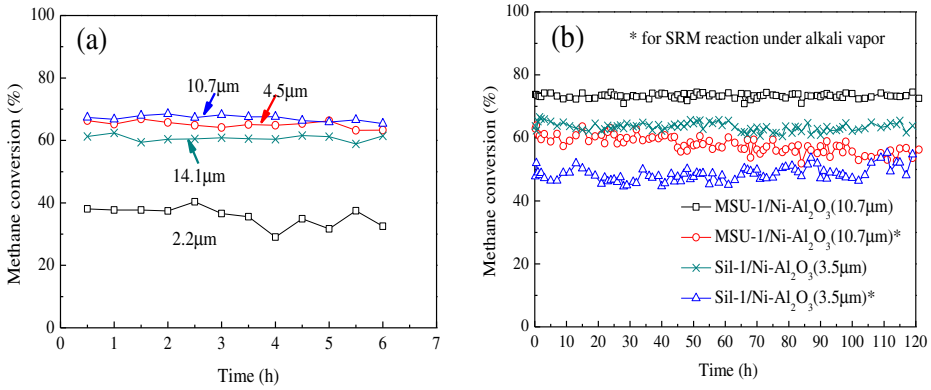

Fig. 10. Catalytic performances of (a) Ni/Al_2O_3-MSU1-A catalysts with different shell thicknesses and (b) the catalysts for SRM reaction over 120 h of reaction.

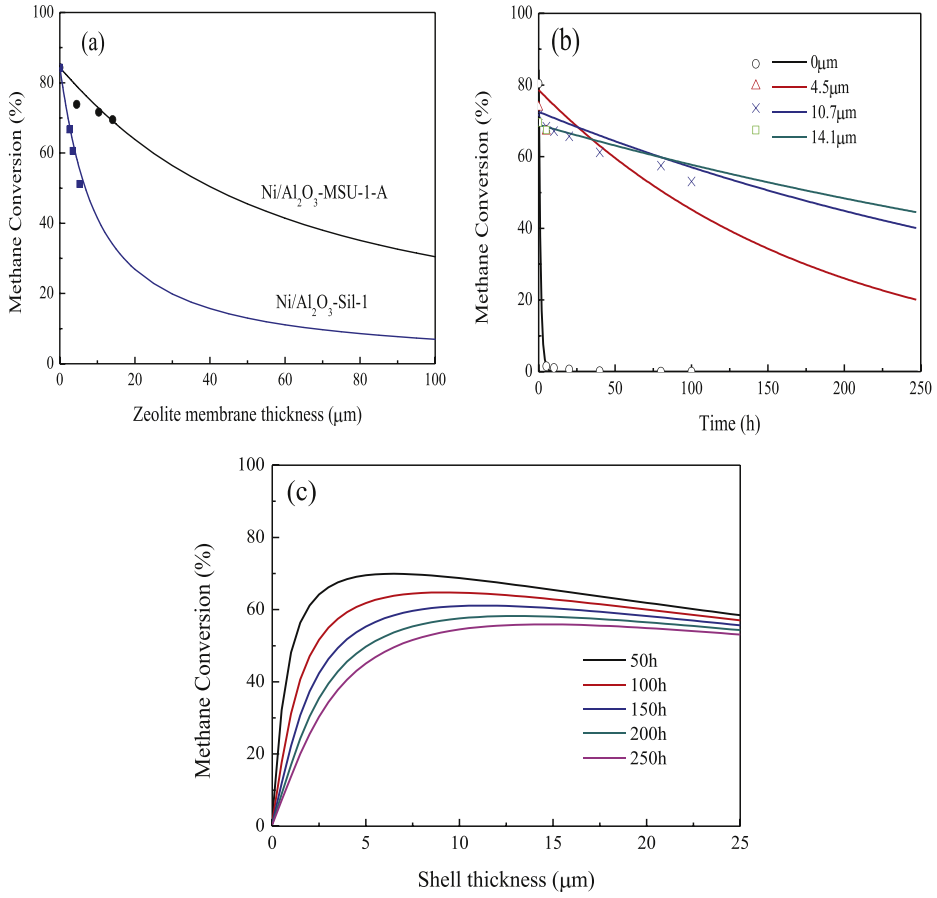

Fig. 11. Plots of methane conversion over (a) fresh MSU-1 and Sil-1 core–shell catalysts with different shell thicknesses, (b) nickel and nickel core–shell catalysts with time exposure to the electrolyte vapors, and (c) time-averaged methane conversion for different shell thicknesses after exposure to 50, 100, 150, 200 and 250 h exposure to the electrolyte vapor (Please note symbols denote experimental data and lines refer to mathematical modeling.).

deactivated within an hour of reaction. The core–shell catalysts are more resistant to alkali poisoning, and catalyst deactivation is less for thicker shells. Model calculations in Fig. 11c predict that a Ni/Al_2O_3-MSU-1-A shell thickness of ca. 15 microns should be considered if the catalyst is to survive 250 h of operation under high alkali conditions following a failure of the anode barrier in a DIR-MCFC. The core–shell catalyst with this shell thickness had a conversion that is within 90% that of the bare Ni/Al_2O_3 catalyst and suffered less than 20% drop in methane conversion and hydrogen yield during 250 h exposure to the alkali poison. A ten micron thick shell similar to the core–shell catalyst shown in Fig. 10b can tolerate exposure to a high concentration of alkali poison for 100 h, sufficient time to carry out necessary repair on the damaged DIR-MCFC.

4. Concluding remarks

This work demonstrates that mesoporous MSU-1 shell with large, inter-connected mesopores could address the shortcomings of the microporous Sil-1 shell, without compromising the core–shell catalyst's ability to resist alkali poisoning under the harsh operating conditions of the DIR-MCFC. Stable methane conversion and hydrogen production could be maintained for at least 100 h under conditions that simulate failure of the anode barrier and direct exposure of the catalysts to hot alkali vapors from the electrolyte. It has also been shown that mathematical modeling can be used to identify the optimum thickness of the MSU-1 shell for a given performance objective. New synthesis method has been developed for preparing low defect MSU-1 shells on the nickel catalyst beads using Sil-1 zeolites as linkers with NaF salts stored in the beads to localize the growth of the MSU-1 shell on the bead surface. This method allowed precise control of the shell thickness and also appeared to moderate the strain caused by the high curvature surface of the bead. It would be important in the following study to investigate the thermomechanical properties of the new core–shell catalysts under practical conditions.

Acknowledgment

This work was supported by China NNSF (No. 21173030, 21036006), Program for Liaoning Excellent Talents in University (Grant No. LR201008) and China National 863 Programme (Grant No. 2007AA05Z137).

References

[1] S.H. Joo, J.Y. Park, C.-K. Tsung, Y. Yamada, P. Yang, G.A. Somorjai, Nat. Mater. 8 (2009) 126–131.
[2] Y. Yoneyama, X.G. San, T. Iwai, N. Tsubaki, Energy Fuels 22 (2008) 2873–2876.
[3] G.H. Yang, Y.S. Tan, Y.Z. Han, J.S. Qiu, N. Tsubaki, Catal. Commun. 9 (2008) 2520–2524.
[4] G.H. Yang, T. Montree, V. Tharapong, N. Tsubaki, Catal. Today 171 (2011) 229–235.
[5] J. Bao, G. Yang, C. Okada, Y. Yoneyama, N. Tsubaki, Appl. Catal. A 394 (2011) 195–200.
[6] G. Yang, N. Tsubaki, J. Shamoto, Y. Yoneyama, Y. Zhang, J. Am. Chem. Soc. 132 (2010) 8129–8136.
[7] X. Li, Y. Zhang, M. Meng, G. Yang, X. San, M. Takahashi, N. Tsubaki, J. Membr. Sci. 347 (2010) 220–227.

[8] N. Nishiyama, K. Ichioka, M. Miyamoto, Y. Egashira, K. Ueyama, L. Gora, W.D. Zhu, F. Kapteijn, J.A. Moulijn, Microporous Mesoporous Mater. 83 (2005) 244–250.
[9] E.E. McLeary, J.C. Jansen, F. Kapteijn, Microporous Mesoporous Mater. 90 (2006) 198–220.
[10] E.A. Khan, A. Rajendran, Z.P. Lai, Ind. Eng. Chem. Res. 49 (2010) 12423–12428.
[11] K.L. Yeung, J.M. Sebastian, A. Varma, J. Membr. Sci. 131 (1997) 9–28.
[12] K.L. Yeung, R. Aravind, R.J.X. Zawada, J. Szegner, G. Cao, A. Varma, Chem. Eng. Sci. 49 (1994) 4823–4838.
[13] K.L. Yeung, A. Gavriilidis, A. Varma, M.M. Bhasin, J. Catal. 174 (1998) 1–12.
[14] J. Zhang, X.F. Zhang, M. Tu, W.F. Liu, H.O. Liu, J.S. Qiu, L. Zhou, Z.G. Shao, H.L. Ho, K.L. Yeung, J. Power Sources 198 (2012) 14–22.
[15] J.L. Zhou, X.F. Zhang, J. Zhang, H.O. Liu, L. Zhou, K.L. Yeung, Catal. Commun. 10 (2009) 1804–1807.
[16] A. Stephen, B.E. Prouzet, T.J. Pinnavaia, Science 269 (1995) 1242–1244.
[17] E. Prouzet, T.J. Pinnavaia, Angew. Chem. Int. Ed. Engl. 36 (1997) 516–518.
[18] S.S. Kim, W.Z. Zhang, T.J. Pinnavaiaa, Science 282 (1998) 1302–1305.
[19] P. Wu, H. Sugiyama, T. Tatsumi, Stud. Surf. Sci. Catal. 146 (2003) 613–616.
[20] É. Prouzet, C. Boissière, C. R. Chim. 8 (2005) 579–596.
[21] K. Maeda, K. Ichinose, T. Yamazaki, T. Suzuki, Microporous Mesoporous Mater. 112 (2008) 603–611.
[22] Z.Y. Sun, Y.Q. Li, T.S. Zhou, Y. Liu, G.Y. Shi, L.T. Jin, Talanta 74 (2008) 1692–1698.
[23] B.A. McCool, W.J. DeSisto, Ind. Eng. Chem. Res. 43 (2004) 2478–2484.
[24] K. Nakagawa, H. Matsuyama, T. Maki, M. Teramoto, N. Kubota, Sep. Purif. Technol. 44 (2005) 145–151.
[25] C. Boissière, M.A.U. Martines, P.J. Kooyman, T.R. Kruijff, A. Larbot, E. Prouzet, Chem. Mater. 15 (2003) 460–463.
[26] C. Boissière, M.U. Martines, A. Larbot, E. Prouzetl, J. Membr. Sci. 25 (2005) 17–28.
[27] N. Jiang, G.H. Yang, X.F. Zhang, L. Wang, C.Y. Shi, N. Tsubaki, Catal. Commun. 12 (2011) 951–954.
[28] K. Katsumi, J. Membr. Sci. 96 (1994) 59–89.
[29] X.B. Wang, X.F. Zhang, Y. Wang, H.O. Liu, J.S. Qiu, J.Q. Wang, W. Han, K.L. Yeung, Chem. Mater. 23 (2011) 4469–4479.
[30] X.B. Wang, X.F. Zhang, Y. Wang, H.O. Liu, J.Q. Wang, J.S. Qiu, H.L. Ho, W. Han, K.L. Yeung, Chem. Eng. J. 175 (2011) 408–416.
[31] X.B. Wang, X.F. Zhang, Y. Wang, H.O. Liu, J.S. Qiu, J.Q. Wang, W. Han, K.L. Yeung, ACS Catal. 1 (2011) 437–445.
[32] X.B. Wang, X.F. Zhang, H.O. Liu, K.L. Yeung, J.Q. Wang, Chem. Eng. J. 156 (2010) 562–570.
[33] Y. Guo, X.F. Zhang, H.Y. Zou, H.O. Liu, J.Q. Wang, K.L. Yeung, Chem. Commun. 39 (2009) 5898–5900.
[34] F.R. Qiu, X.B. Wang, X.F. Zhang, H.O. Liu, S.Q. Liu, K.L. Yeung, Chem. Eng. J. 147 (2009) 316–322.
[35] K.Y. Seok, Y.S. Man, Adv. Mater. 14 (2002) 1078–1081.
[36] K.F. Lam, H. Kassab, M. Pera-Titus, J. Phys. Chem. C 115 (2011) 176–187.
[37] L.T.Y. Au, J.L.H. Chau, C.T. Ariso, K.L. Yeung, J. Membr. Sci. 183 (2001) 269–291.
[38] J.L.H. Chau, A.Y.L. Leung, K.L. Yeung, Lab Chip 3 (2003) 53–55.
[39] Y. Liu, W.Z. Zhang, T.J. Pinnavaia, Angew. Chem. Int. Ed. 40 (2001) 1255–1258.
[40] E.R. Geus, H. van Bekkum, Zeolites 15 (1995) 333–341.
[41] A.C. Voegtlin, F. Ruch, J.L. Guth, J. Patarin, L. Huve, Microporous Mater. 9 (1997) 95–105.
[42] P.T. Tanev, T.J. Pinnavaia, Science 267 (1995) 865–867.
[43] Iler, K. Ralph, The Chemistry of Silica – Solubility, Polymerization, Colloid and Surface Properties and Biochemistry, Wiley, New York, 1979.